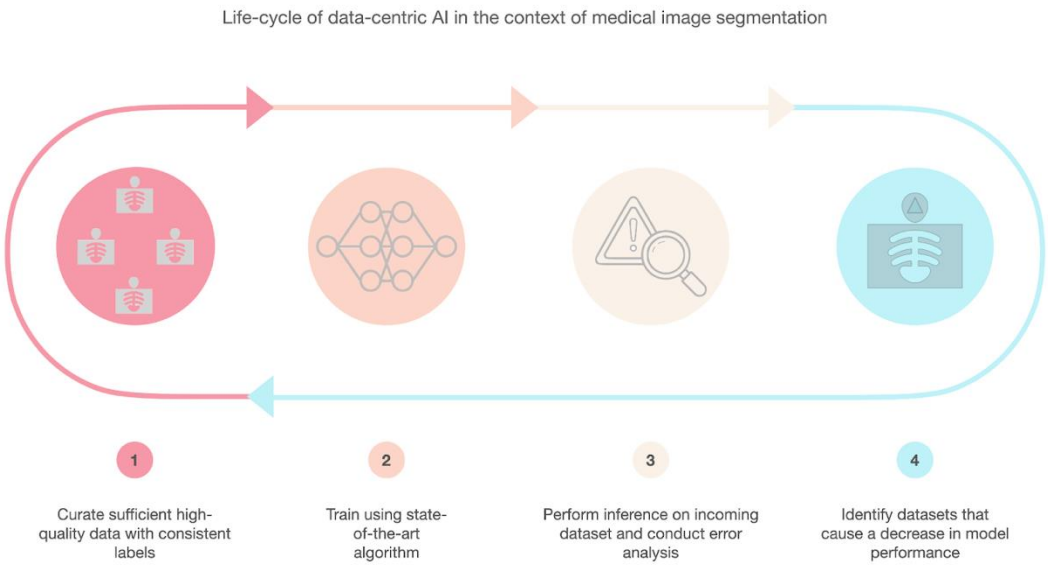

Supplemental Figure 1. Life-cycle of data-centric AI approach. The main goal is to identify the datasets that cause a reduction in the model's performance. Once these datasets are identified, they are added to the original training dataset, and the network is retrained.

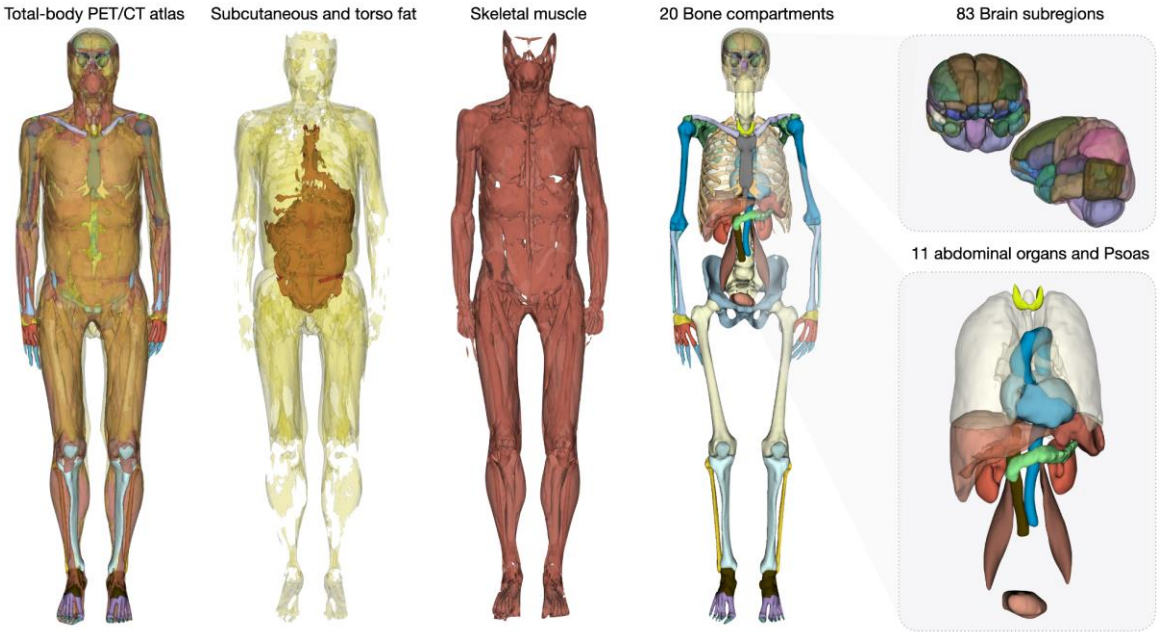

Supplemental Figure 2. ^{18}F-FDG total-body PET/CT tissue-map consisting of 120 unique tissues - both cerebral and non-cerebral structures.

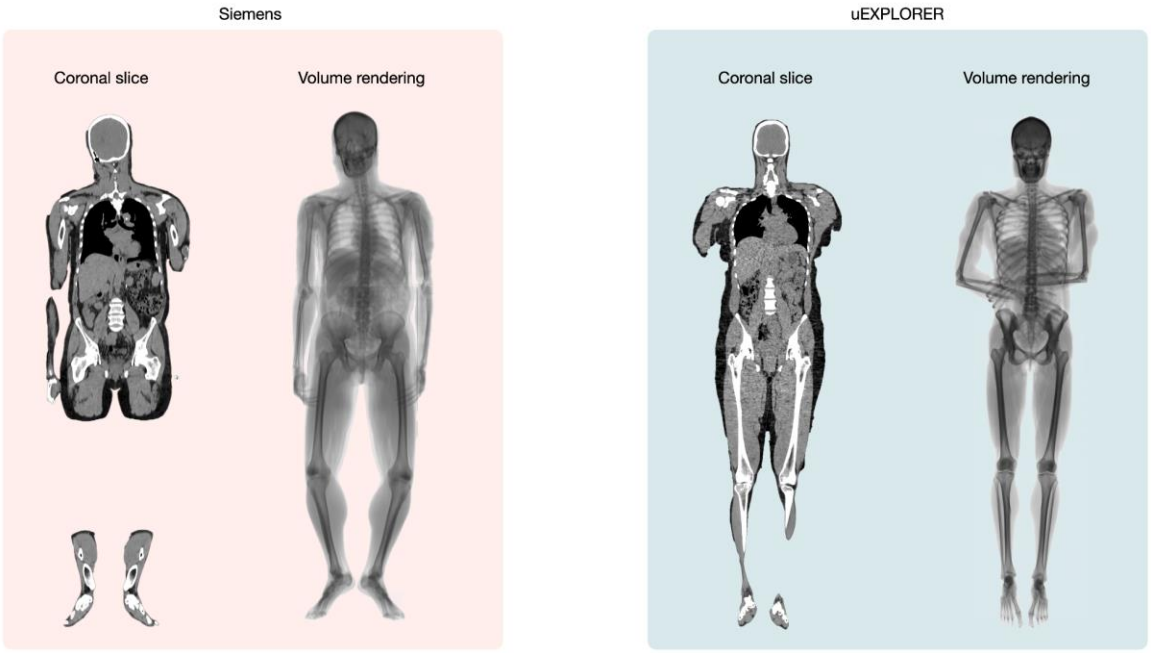

Supplemental Figure 3. An example image of a low-dose CT from the Siemens (left) and uEXPLORER (right) system. The two images differ in their noise characteristics and the hand-positions of the subjects. Subjects scanned using the Siemens system position their hands side-by-side (left), while subjects scanned using the uEXPLORER system have their hands crossed across the chest (right).

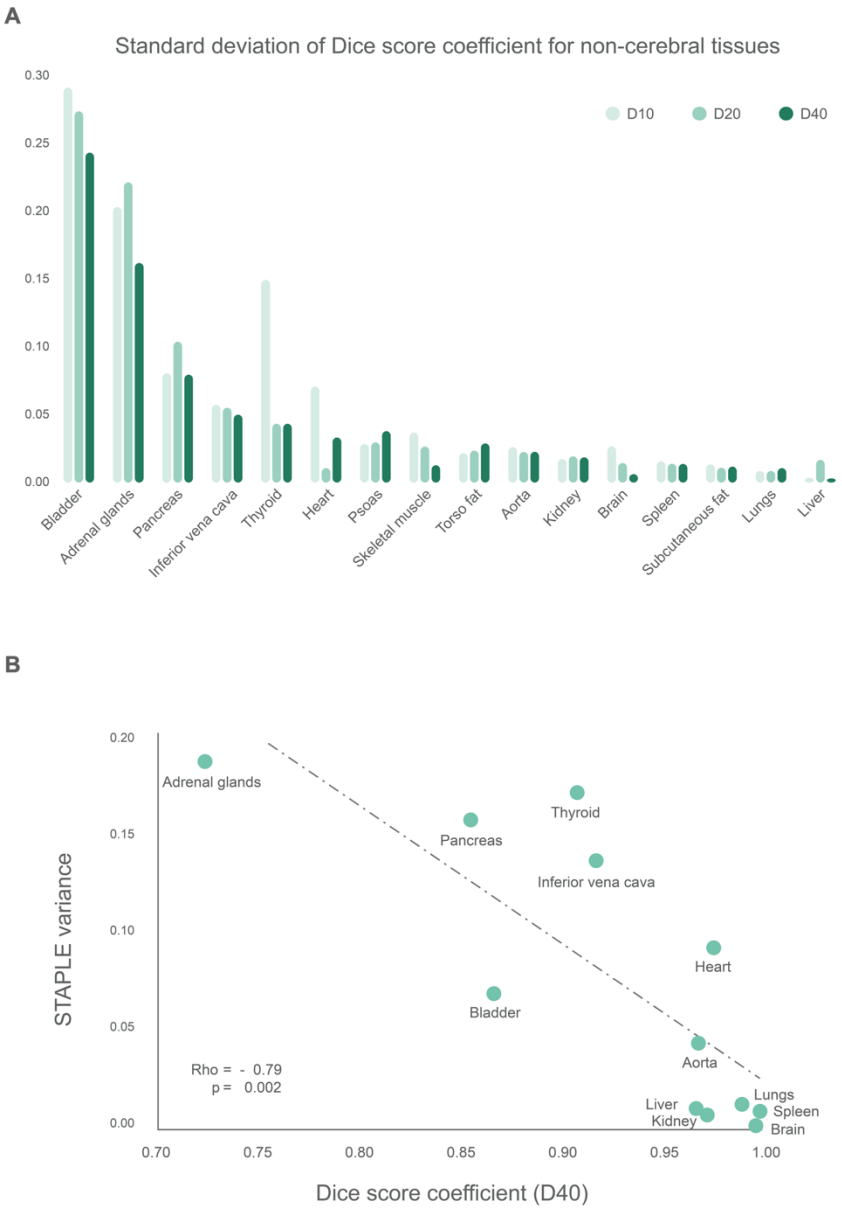

Supplemental Figure 4. **(A)** Standard deviation (SD) values of Dice Score Coefficients (DSCs) were determined for various abdominal organs derived using 10 (D10), 20 (D20) and 40 (D40) training datasets. The graph indicates that SD values are similar for most organs except for the bladder, adrenal gland, thyroid and pancreas. **(B)** The correlation plot shows a highly significant negative correlation between the DSCs obtained from the D40 training dataset and the STAPLE variance. The organs with the lowest DSC values are also those with the highest SD (adrenal gland, pancreas and thyroid), indicating that segmentation of these three structures is problematic even for human experts.

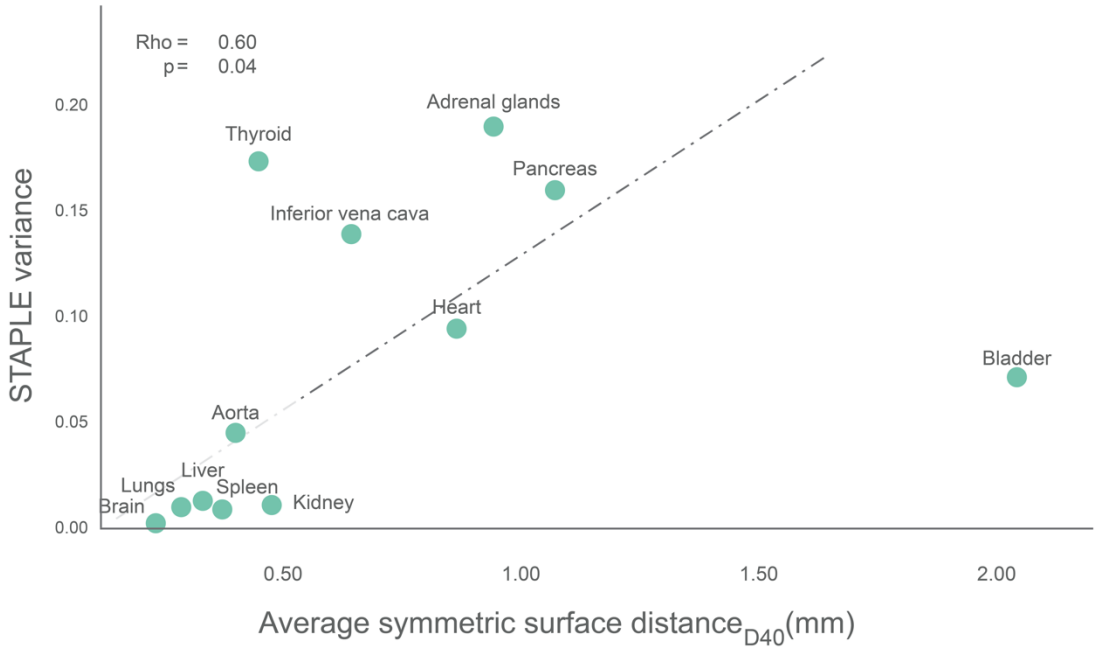

Supplemental Figure 5. The correlation plot shows a significant correlation between the average symmetric surface distance (ASSD) and the STAPLE variance, indicating that the segmentation of the bladder, pancreas and the adrenal gland is more challenging than for other organs. It can be seen that the average misalignment between contours is about twice (>1mm) that of other organs, confirming the conclusion derived using the DSC metric.

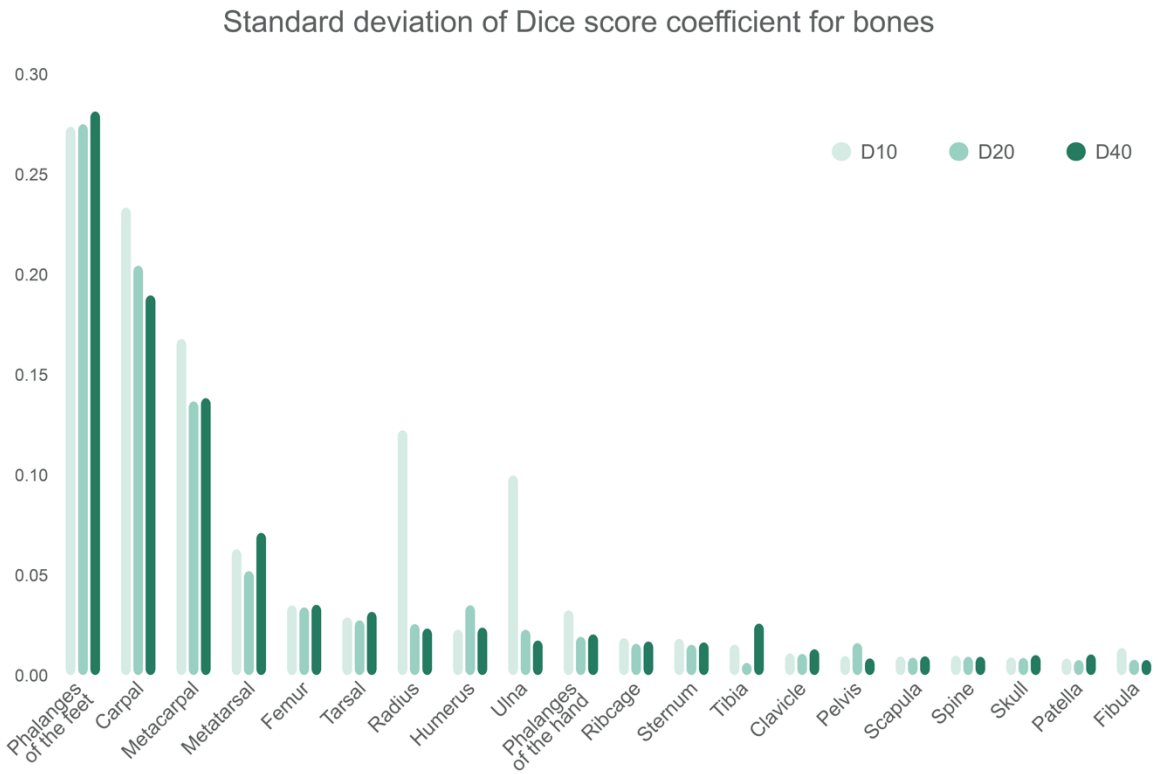

Supplemental Figure 6. Standard deviation (SD) values of Dice Score Coefficients (DSCs), determined for various bone structures derived using 10 (D10), 20 (D20) and 40 (D40) training data sets. The graph indicates that the SD of the three data sets is similar for most organs, except for the radius and ulna. The variability in segmentation accuracy of these two bone structures is high in case of a small training data.

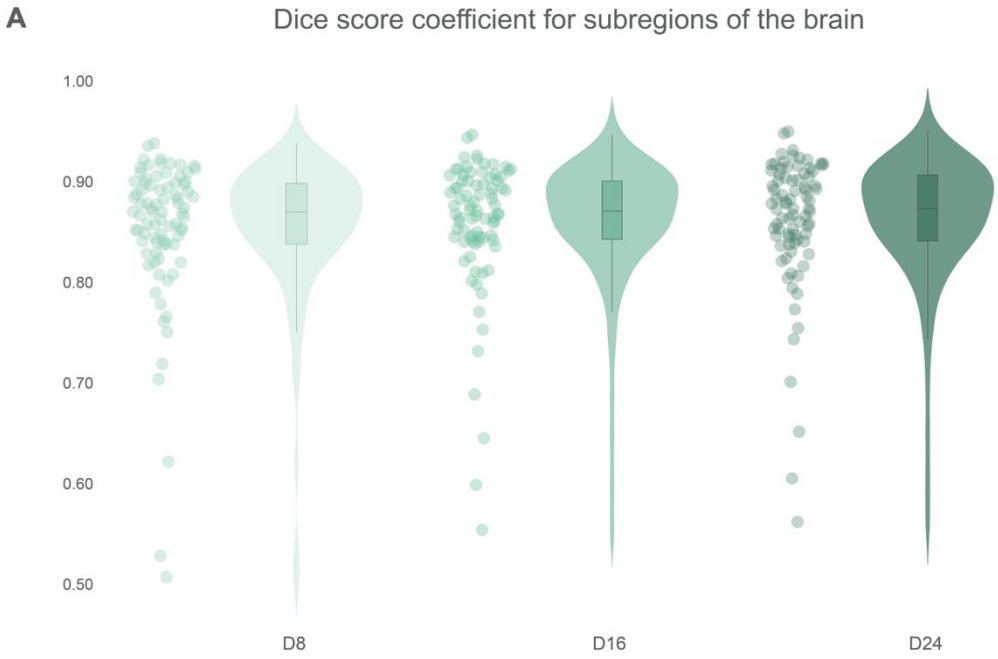

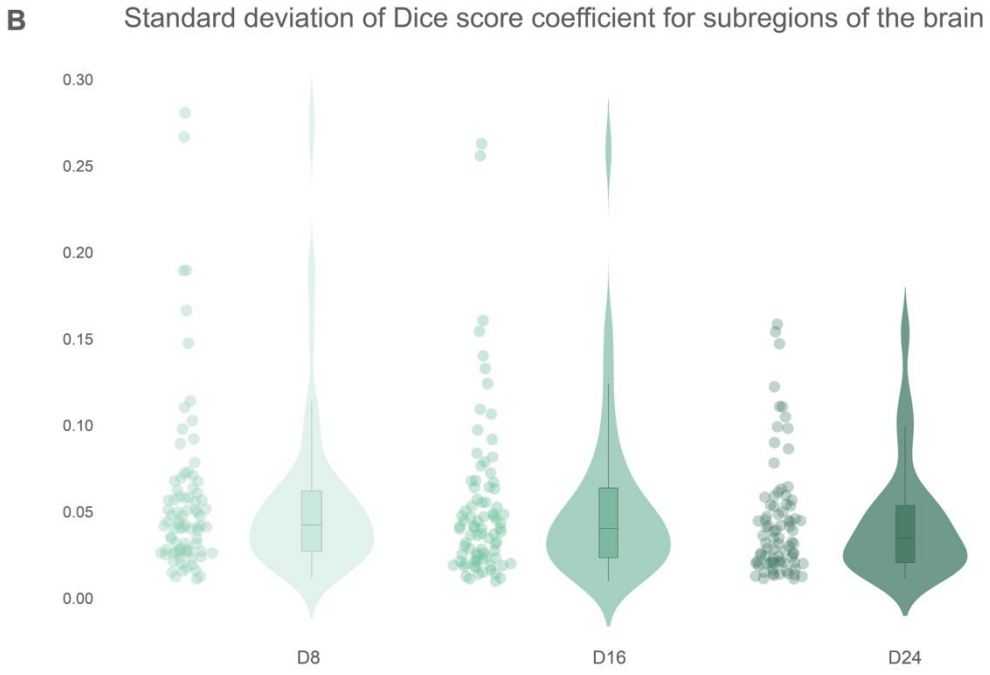

41

42 **Supplemental Figure 7**. Mean (A) and SD (B) values of the DSCs determined for various brain regions
43 (denoted by dots) derived using 8 (D8), 16 (D16) and 24 (D24) training datasets. One can appreciate that
44 increase in the training data set size has only a minor effect on segmentation performance, causing a small
45 decrease in the DSC variance.

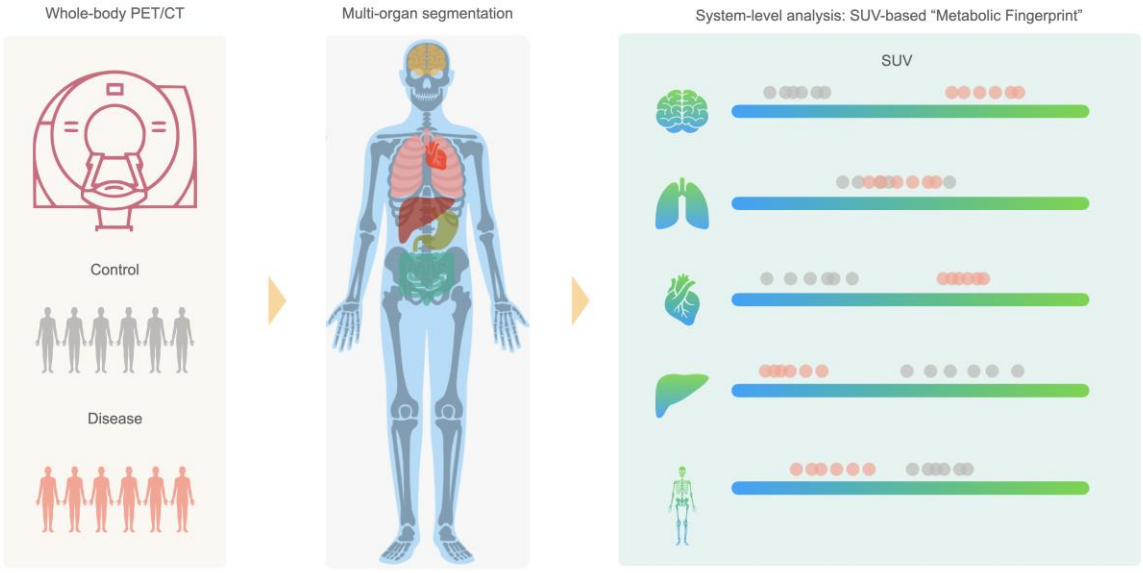

Supplemental Figure 8. Concept diagram showing the extraction of a "metabolic fingerprint" from PET/CT data obtained from a control and disease population. The developed automated multi-organ segmentation pipeline is used to extract organ SUV values from both groups (control: grey, disease: orange), allowing the study of systems-level alterations in the pattern of organ metabolic activity as a consequence of the disease process.

SUPPLEMENTAL TABLES

Supplemental Table 1. List of cerebral (highlighted in green) and non-cerebral tissues (highlighted in orange) along with their corresponding label-index in the total-body digital FDG PET/CT tissue-map.

Label-index	Tissues
1	R-Hippocampus
2	L-Hippocampus
3	R-Amygdala
4	L-Amygdala
5	R-Anterior-temporal-lobe-medial-part
6	L-Anterior-temporal-lobe-medial-part
7	R-Anterior-temporal-lobe-lateral-part
8	L-Anterior-temporal-lobe-lateral-part
9	R-Parahippocampal-and-ambient-gyri
10	L-Parahippocampal-and-ambient-gyri
11	R-Superior-temporal-gyrus-posterior-part
12	L-Superior-temporal-gyrus-posterior-part
13	R-Middle-and-inferior-temporal-gyrus
14	L-Middle-and-inferior-temporal-gyrus
15	R-Fusiform-gyrus
16	L-Fusiform-gyrus
17	R-Cerebellum
18	L-Cerebellum
19	Brainstem
20	L-Insula
21	R-Insula
22	L-Lateral-remainder-of-occipital-lobe
23	R-Lateral-remainder-of-occipital-lobe
24	L-Cingulate-gyrus-gyrus-cinguli-anterior-part
25	R-Cingulate-gyrus-gyrus-cinguli-anterior-part
26	L-Cingulate-gyrus-gyrus-cinguli-posterior-part
27	R-Cingulate-gyrus-gyrus-cinguli-posterior-part

28	L-Middle-frontal-gyrus
29	R-Middle-frontal-gyrus
30	L-Posterior-temporal-lobe
31	R-Posterior-temporal-lobe
32	L-Inferiolateral-remainder-of-parietal-lobe
33	R-Inferiolateral-remainder-of-parietal-lobe
34	L-Caudate-nucleus
35	R-Caudate-nucleus
36	L-Nucleus-accumbens
37	R-Nucleus-accumbens
38	L-Putamen
39	R-Putamen
40	L-Thalamus
41	R-Thalamus
42	L-Pallidum
43	R-Pallidum
44	Corpus-callosum
45	R-Lateral-ventricle-excluding-temporal-horn
46	L-Lateral-ventricle-excluding-temporal-horn
47	R-Lateral-ventricle-temporal-horn
48	L-Lateral-ventricle-temporal-horn
49	Third-ventricle
50	L-Precentral-gyrus
51	R-Precentral-gyrus
52	L-Straight-gyrus
53	R-Straight-gyrus
54	L-Anterior-orbital-gyrus
55	R-Anterior-orbital-gyrus
56	L-Inferior-frontal-gyrus
57	R-Inferior-frontal-gyrus
58	L-Superior-frontal-gyrus
59	R-Superior-frontal-gyrus
60	L-Postcentral-gyrus

61	R-Postcentral-gyrus
62	L-Superior-parietal-gyrus
63	R-Superior-parietal-gyrus
64	L-Lingual-gyrus
65	R-Lingual-gyrus
66	L-Cuneus
67	R-Cuneus
68	L-Medial-orbital-gyrus
69	R-Medial-orbital-gyrus
70	L-Lateral-orbital-gyrus
71	R-Lateral-orbital-gyrus
72	L-Posterior-orbital-gyrus
73	R-Posterior-orbital-gyrus
74	L-Substantia-nigra
75	R-Substantia-nigra
76	L-Subgenual-frontal-cortex
77	R-Subgenual-frontal-cortex
78	L-Subcallosal-area
79	R-Subcallosal-area
80	L-Pre-subgenual-frontal-cortex
81	R-Pre-subgenual-frontal-cortex
82	L-Superior-temporal-gyrus-anterior-part
83	R-Superior-temporal-gyrus-anterior-part
84	Adrenal-glands
85	Aorta
86	Bladder
87	Brain
88	Heart
89	Kidneys
90	Liver
91	Pancreas
92	Spleen

93	Thyroid
94	Inferior vena cava
95	Lung
96	Carpal
97	Clavicle
98	Femur
99	Fibula
100	Humerus
101	Metacarpal
102	Metatarsal
103	Patella
104	Pelvis
105	Phalanges of the hand
106	Radius
107	Ribcage
108	Scapula
109	Skull
110	Spine
111	Sternum
112	Tarsal
113	Tibia
114	Phalanges of the feet
115	Ulna
116	Skeletal-muscle
117	Subcutaneous-fat
118	Torso-fat
119	Psoas
120	Entire Skeleton